J. Marine. Sci. Appl. (2009) 8: 110-116
DOI: 10.1007/s11804-009-8110-4

Three-dimensional numerical simulation of the flow past a circular cylinder based on LES method

CHEN Hai-long*, DAI Shao-shi, LI Jia and YAO Xiong-liang

College of Shipbuilding Engineering, Harbin Engineering University, Harbin 150001, China

Abstract: The hydrodynamic characteristics of a rigid, single, circular cylinder in a three dimensional, incompressible, uniform cross flow were calculated using the large-eddy simulation method of CFX5. Solutions to the three dimensional N-S equations were obtained by the finite volume method. The focus of this numerical simulation was to research the characteristics of pressure distribution (drag and lift forces) and vortex tubes at high Reynolds numbers. The results of the calculations showed that the forces at every section in the spanwise direction of the cylinder were symmetrical about the middle section and smaller than the forces calculated in two dimensional cases. Moreover, the flow around the cylinder obviously presents three dimensional characteristics.

Keywords: LES method; three-dimensional flow past circular cylinder; hydrodynamic characteristics
CLC number: O35 **Document code:** A **Article ID:** 1671-9433(2009)02-0110-07

1 Introduction

The phenomenon of flow around a cylinder has been paid with widespread attention since 1960s and a large number of studies have been published. But due to the restriction of theory, experimental condition and other facts, most of the experiments were hard to be carried out when Reynolds number was high. With the speed and capacity of computer increasing rapidly, simulation technology is getting more and more sophisticated, and simulation research has become an effective means of turbulence research.

At present many scholars at home and abroad have carried out in-depth research in 2-D flow around a cylinder. But there are few articles published about the research of 3-D flow around a cylinder. 3-D incompressible and viscous flow around a cylinder is simulated by finite volume method and SIMPLE calculation format (*Re*=1 000, *Re*=10 000 respectively). They found that the fluid around the cylinder had obvious 3-D characteristics when the Reynolds number was high. The 3-D flow around a cylinder in large eddy simulation (LES) (*Re*=14 000) is simulated. It showed that 3-D simulations about flow around a cylinder in LES were much close to experimental results. The 3-D simulation about cylindrical vortex-induced vibration that has 2 degree of freedom and the simulation results were much close to the results that Achenbach and Schewe had calculated.

Received date: 2009-02-27.
***Corresponding author Email:** chenhailong@hrbeu.edu.cn

2 Mathematical model

2.1 Controlling equations

This article adopts advanced turbulent model LES to numerically simulate the hydrodynamic characteristics of the rigid isolated cylinder.

The model LES mostly uses the method of filtering to decompose the vortex in the wakes into a large scale one and a small scale one, and then numerically solves them and calculates them respectively. The model LES is to decompose the flow variables in the flow fields into a large scale one (solvable) and a small scale one (unsolvable, used to simulate with SGS model). For an arbitrary transient, the fluid variable f is written as: $f = \overline{f} + f'$. The large scale variable after filtering is

$$\bar{f}(x_i,t) = \int_V G(x_i - x_i')f(x_i',t)\mathrm{d}x_i', \qquad (1)$$

where $\overline{f}$ is a large-scale variable, and is defined by volume-averaged; f' is a small-scale variable reflecting the small-scale movement's contribution for f. It is also named as Sub-grid-scale Component.

$G(x_i - x_i')$ is the Gaussian filter. The 3-D incompressible Navier-Stokes equation is filtered, and the model SGS is introduced to write it as follows:

$$\nabla \cdot u = 0, \qquad (2)$$

$$\frac{\partial \rho \overline{u_i}}{\partial t} + \frac{\partial}{\partial x_j}(\rho \overline{u_i u_j}) = -\frac{\partial p}{\partial x_i} + \mu \frac{\partial^2 \overline{u_i}}{\partial x_j x_j} + \frac{\partial \tau_{ij}}{\partial x_j}, \qquad (3)$$

$$\tau_{ij} = \nu_{\mathrm{SGS}} \cdot \left(\frac{\partial \bar{u}_i}{\partial x_j} + \frac{\partial \bar{u}_j}{\partial x_i}\right), \tag{4}$$

where $\bar{u}$ and $\bar{v}$ are the velocity along *x*-axis and the velocity along *y*-axis in the Cartesian coordinate system after filtering respectively, $\bar{p}$ is the pressure in the Cartesian coordinate system; τ_{ij} is the unsolved sub-grid-scale turbulent stress; ν_{SGS} is the sub-grid-scale eddy viscosity coefficient; $\nu_{\mathrm{SGS}} \propto l q_{\mathrm{SGS}}$, $l = \Delta = V^{1/3}$, Δ is the gird width; q_{SGS} is the unsolved velocity.

$$q_{SGS} = \Delta \left|\bar{S}\right| = \Delta \left(2\bar{S}_{ij}\,\bar{S}_{ij}\right)^{1/2}.$$

$$\tau_{ij} = (C_S \Delta)^2 \bar{S}, \tag{5}$$

where C_S is the Smagorinsky constant, here $C_S = 0.1$. Eq.(4) is substituted into Eq.(3) to solve Eqs.(2) and (3).

2.2 Initial conditions and boundary conditions

In order to solve the motion equation of the viscous fluid better, the initial conditions and the boundary conditions of the flow field must be defined. There is no slip at the interface between fluid and solid on the rigid column wall surface, that is $u_n = 0$. The initial conditions of the unsteady viscous fluid are first, the reference pressure of the flow field is 1 atm, and second the water temperature is 15℃. The velocity of the uniform flow at infinite point of the flow field is u_∞. The far field condition is that at infinite point of the flow field (the export of the flow field), the average static pressure $p = 0$.

2.3 The establishment of the model and the grid divisions

Ref.[1] shows that when the spanwise length of the cylinder $Z \geq \pi D$, the cylinder's flow problems will present obvious three-dimensional effect. According to Refs.[2-6], the dimension and the arrangement mode of the computational flow field are determined as Fig.1. Unstructured meshes (Hex8) are adopted to mesh the whole flow field. The computational domain is divided into 9 regions. Near the wall of the cylinder, the mesh is dense, and in other regions, the mesh becomes sparser gradually. The numbers of the spanwise meshes and the computational meshes are 50 and 944 000 respectively.

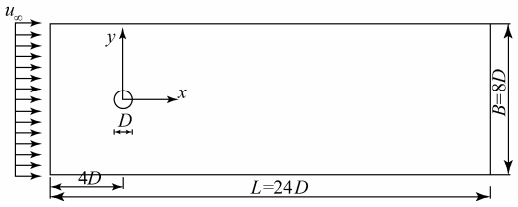

(a) Planform of arrangement

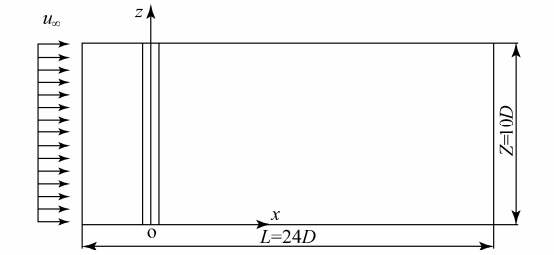

(b) Left elevation of arrangement

Fig.1 Arrangement of the computational flow field

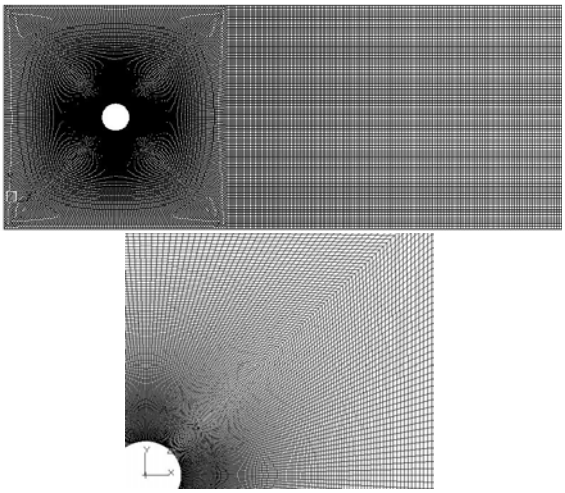

Fig.2 Schematic diagram of the meshing plan

3 The definition of the dimensionless parameters

3.1 The stable pressure coefficients and the fluctuating pressure coefficients

$$C_{p0}(\theta) = \frac{P_0(\theta) - P_\infty}{1/2 \cdot \rho \cdot u_\infty^{\,2}}, \tag{6}$$

$$C_p'(\theta,t) = \frac{P'(\theta,t)}{1/2 \cdot \rho \cdot u_\infty^{\,2}}, \tag{7}$$

where $p_0(\theta)$ and $p'(\theta,t)$ are the stable pressure and the fluctuating pressure at each measuring point of the cylinder surface, respectively; p_∞, u_∞, ρ are the hydrostatic pressure, the free stream velocity and the density of the fluid at infinite point.

3.2 The stable lift coefficients and resistance coefficients and the fluctuating ones at each section of the cylinder

$$C_{do} = \frac{1}{2}\int_0^{2\pi} C_{p0}(\theta)\cos\theta \mathrm{d}\theta, \tag{8}$$

$$C_{lo} = \frac{1}{2}\int_0^{2\pi} C_{p0}(\theta)\sin\theta \mathrm{d}\theta, \tag{9}$$

$$C_l'(t) = \frac{1}{2}\int_0^{2\pi} C_p'(\theta,t)\sin\theta \mathrm{d}\theta, \tag{10}$$

$$C_d'(t)=\frac{1}{2}\int_0^{2\pi}C_p'(\theta,t)\cos\theta \mathrm{d}\theta . \quad (11)$$

The definition of θ is shown in Fig.3(a). The fluctuating lift coefficients and the fluctuating resistance coefficients adopt the corresponding root mean square values, $C_l'=\sqrt{\mathrm{E}\left[C_L'(t)\right]^2}$, $C_d'=\sqrt{\mathrm{E}\left[C_d'(t)\right]^2}$.

3.3 The lift coefficients and the resistance coefficients of the whole cylinder

$$C_l(t)=\frac{F_l(t)}{1/2\cdot\rho\cdot V^2 HD}, \quad (12)$$

$$C_d(t)=\frac{F_d(t)}{1/2\cdot\rho\cdot V^2 HD}, \quad (13)$$

where $F_l(t)$ and $F_d(t)$ are the lift and the resistance (N) on the whole cylinder; H are the spanwise height of the cylinder. C_l' and C_d' also adopt the root mean square values, and their algorithm is the same as above.

4 Numerical results

Pressure sensing points are arranged every 15 degrees in the circumferential direction of the cylinder, and five pressure sensing surfaces are arranged in the spanwise direction of the cylinder, and a detailed analysis of the distribution law of the stable pressure coefficients and the fluctuating pressure coefficients of each pressure sensing surface are shown in Fig.3. The height from each section to the origin is adopted to define the section.

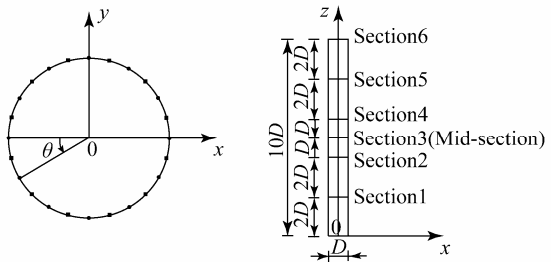

Fig.3 Pressure sensing points and surfaces of the cylinder

4.1 The circumferential distribution of the cylinder's stable and fluctuating pressure coefficients

In Fig.4(a), C_{p0} is the maximum value at the stagnation point of the cylinder (θ=0º or 360º), about 0.9. With the inflow's extension to both sides of the cylinder, C_{p0} reduces to its minimum rapidly. When $\theta=60^\circ$ or $\theta=300^\circ$, it is about -1.8. It is between -1.0 and -1.2 in the back pressure region. In Fig.4(b), C_p' is the minimum value at the stagnation point of the cylinder, about 0.011. When $\theta=90^\circ$ and $\theta=270^\circ$, respectively, the symmetric peak turns up, and then decreases to a flat value. But on this condition, changes of fluctuating pressure coefficients at different sections are not the same. Second peaks of section 1 and section 2 appear when $\theta=195^\circ$, and small peak of section 3 appears when $\theta=180^\circ$, while changes of section 4 and section 5 in this region are not obvious. When θ is the same, Ref.[7] gives the two-dimensional experimental results of the flow around cylinder. The maximum value of C_{p0} is 1.0 when θ=0º or 360º, and its minimum value is about -1.6, and in the back pressure region C_{p0} is about -1.2. The peak of C_p' appears when θ=75º or 285º, and its minimum is about 0.1. C_{p0} and C_p' obtained in the numerical experiment of the three-dimensional flow around cylinder are all slightly smaller than those in the two-dimensional experiment. C_{p0} at each section has no significant change, while C_p' changes greatly.

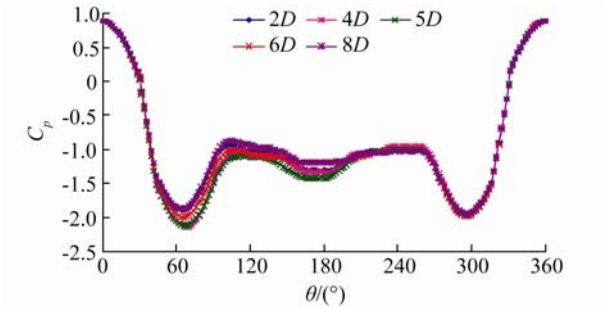

(a) Stable pressure coefficients

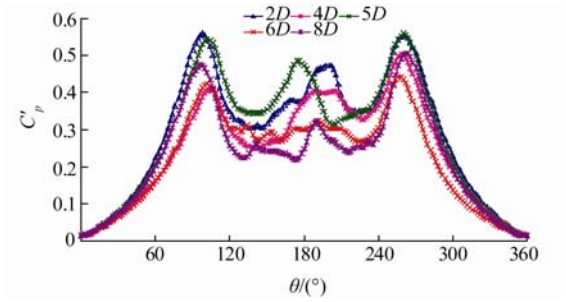

(b) Fluctuating pressure coefficients

Fig.4 The cylinder's stable pressure coefficients at each section and the fluctuating pressure coefficients

4.2 Abscisic point of the vortex and the wake pressure

The definitions of the abscisic point and its detachment angle of the vortex are shown in Fig.5. Changes of the vortex's separation point at each section in the spanwise direction are shown in Fig.6. At each section in the spanwise direction, we lay out a measuring point every 2D from *x*-axis to the central point of the cylinder at that section, then each spanwise section has 10 measuring points, as shown in Fig.5.

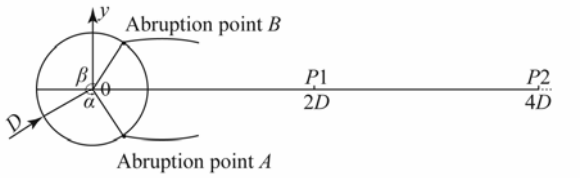

Fig.5 The separation point and measuring points of the section

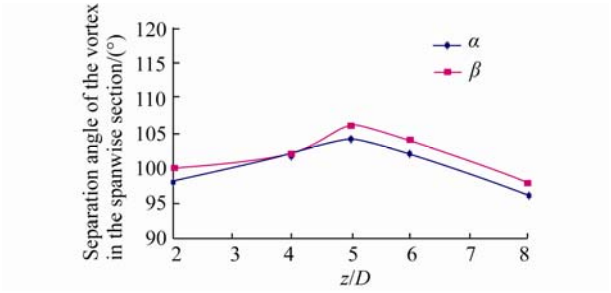

Fig.6 Changes of the separation angle of the vortex in the spanwise section

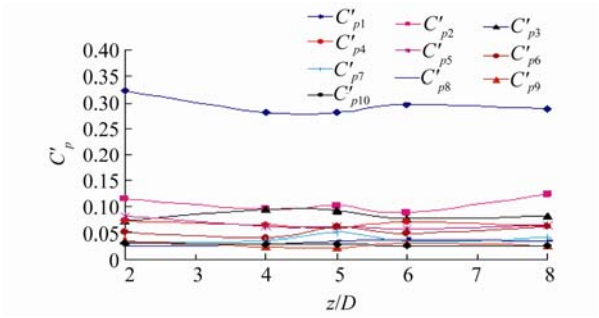

Fig.7 Changes of $C_p^{'}$ in the spanwise section

In Fig.6, the abscisic points of the vortex at different sections are not the same. The abscisic points of the vortex at the five sections in the spanwise direction of the cylinder move to the back pressure region gradually from the end section to the middle section, that is, the vortex's abscisic angle of the middle section are larger than that of the end section, and changes of the vortex's abscisic angles α and β show symmetry in the spanwise direction when fluid flows around three-dimensional cylinder. This suggests that when the Reynolds number and the spanwise length are as above, the flowing around the cylinder shows obvious three-dimensional features.

In Fig.7, $C_p^{'}$ of points in the wake flow region of the cylinder at each spanwise section are larger near the wall of the cylinder, while with the increasing of the distance, the values of $C_p^{'}$ markedly decrease to about zero and show smooth changes. Meanwhile, the values of $C_p^{'}$ of the measuring points near the wall change obviously, and they change very smoothly in the spanwise direction far away from the wall of the cylinder. This suggests that the three-dimensional character of the pressure near the wall of the cylinder is stronger than that far away from the wall. $C_p^{'}$ show obvious two-dimensional character far away from the wall of the cylinder, namely, after $x = 16D$.

4.3 The spanwise distribution of the lift coefficients and the resistance coefficients at each section of the cylinder

The duration curves of the lift coefficients and the resistance coefficients in the spanwise direction at each section of the cylinder are shown in Fig.8. C_{l1} and C_{l2} respectively represent the lift coefficients of section 1 and section 2, and the others are in the same way. C_{l6} and C_{d6} are the lift coefficients and the resistance coefficients of the whole cylinder, respectively.

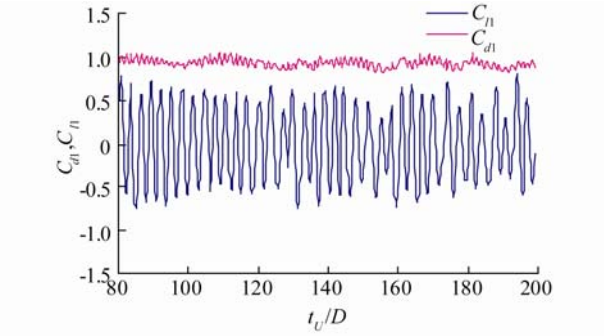

(a) Section 1

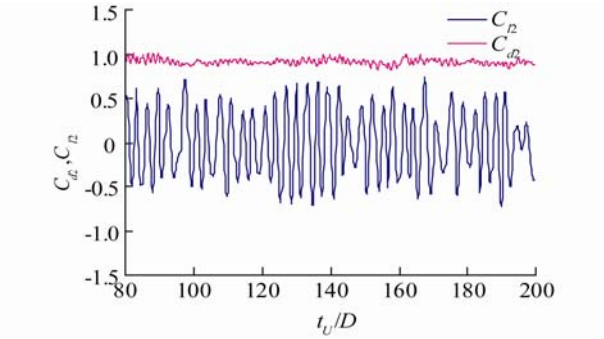

(b) Section 2

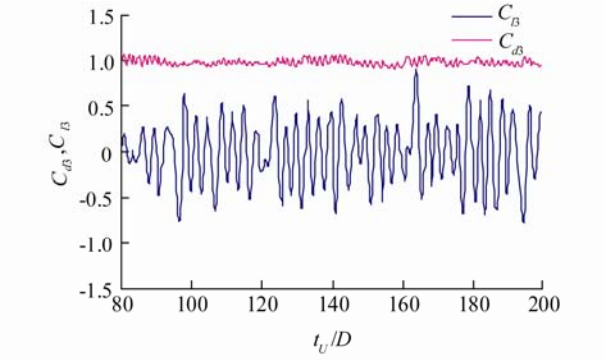

(c) Section 3

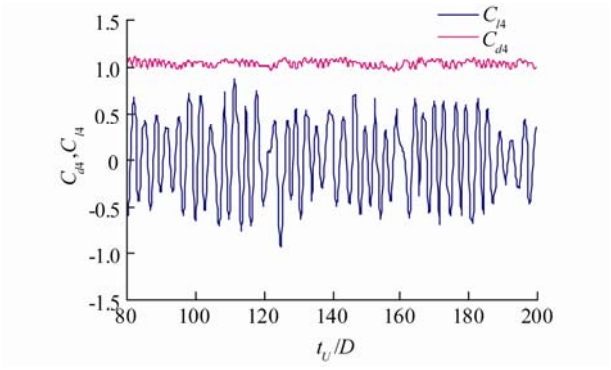

(d) Section 4

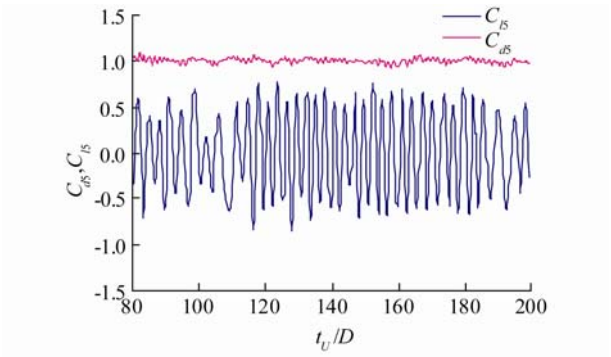

(e) Section 5

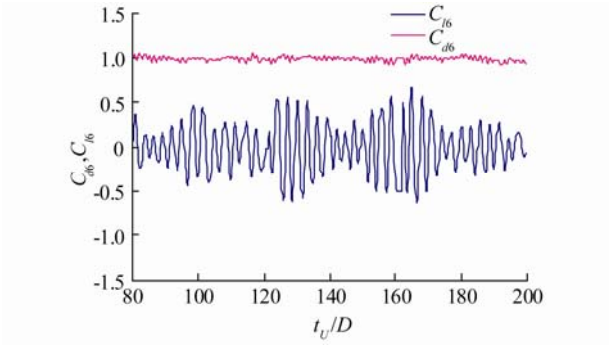

(f) The whole cylinder

Fig.8 Curves of the lift and resistance coefficients

In Fig.8, $C_l(t)$ and $C_d(t)$ are not the same at different sections, but they are symmetrical about the middle section. The symmetry of the flow around shows that C_{l0} is 0. $C_l(t)$ is much larger than $C_d(t)$, so we can see that the effects of the lift on the cylinder are very strong, while the effects of the resistance are very weak. In Fig.9 we can see that C_d and $C_l^{'}$ are symmetrical about the middle section, and their values are the maximum at the middle section, and then they decrease gradually toward the two ends, while the changing trend of $C_d^{'}$ is smooth.

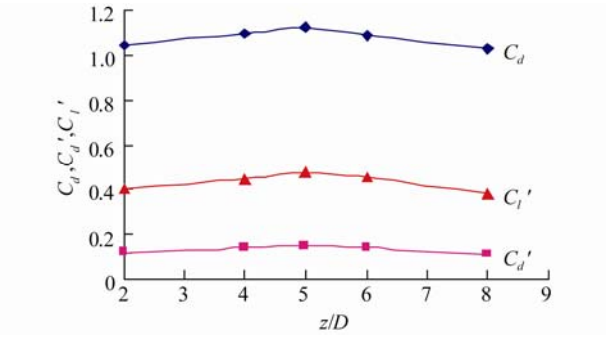

(a) Changes of C_d, C_d', C_l'

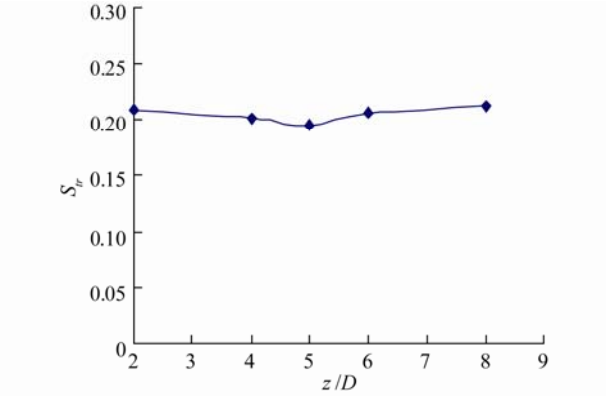

(b) Changes of S_{tr}

Fig.9 Changes of C_d, C_d', C_l' and S_{tr} in the spanwise direction of the cylinder ($Re = 2.2\times10^4$)

Table 1 gives the hydrodynamic parameters of the whole cylinder. By contrast in Table 1, it can be seen that the accuracy of the calculation on the problem of three-dimensional flow around the cylinder using the advanced turbulent model LES is higher, and the calculation error is about 5%.

Table 1 Hydrodynamic parameters of the cylinder

Numerical results	C_{pb}	C_{d0}	C_d'	C_l'
Whole cylinder	- 1.108	1.072	0.132	0.429
Ref.[3]	- 1.129	1.143	—	0.448
Error/%	1.9	6.2	—	4.2

From the analysis above, the three-dimensional character of the flow around the cylinder is non-negligible. But the cylinder is long enough, and the three-dimensional effect on the middle section is the smallest for each section, meanwhile, in Table 2 the hydrodynamic parameters of the middle section and the two-dimensional experiment results are basically identical, so two-dimensional numerical method can be used to simulate the hydrodynamic parameters of the middle section. But from Fig.6 and Fig.9, the hydrodynamic parameters of other sections are significantly different from those of the middle section. So the three-dimensional relativity

problems must be considered when calculating the flow around the cylinder.

Table 2 Hydrodynamic parameters of the mid-section of the 3-D cylinder and the 2-D experimental results

Numerical results	C_{pb}	C_l'	C_{d0}
Mid-section of the cylinder($z = 5D$)	-1.171	0.473	1.127
2-D cylinder experiment results[7]	-1.2	0.5	1.2
Error/%	2.5	5.8	6.5

4.4 Stena-Haar number

Using the lift's adaptive power spectral density function $S(f)$, the Stena-Haar Number is defined as $S_{tr} = \frac{f_s \times D}{u_\infty}$.

The power spectral density functions of the lift and the resistance are shown in Fig.10. The frequency shown on the right side of the picture is the peak value of the curve. The lift changes with the Stena-Haar frequency f_s, and the resistance consists of two parts-stable resistance and fluctuating resistance changing in 2 f_s consistently[8]. S_{tr} is not obvious in the spanwise direction of the cylinder (Fig.9), and is symmetrical about the mid-section. The numerical results are shown in Table 3.

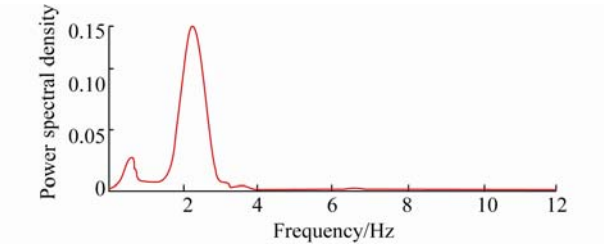

(a) The power spectral density of lift

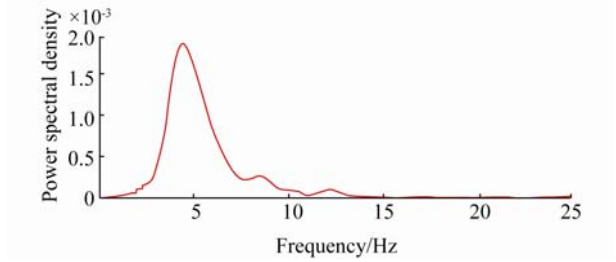

(b) The power spectral density of fluctuating resistance

Fig.10 The power spectral density of lift and fluctuating resistance of the section ($z = 2D$)

Table 3 Contrast table of the calculation results of the whole cylinder's S_{tr}

S_{tr}	LES Numerical results	Ref.[9]	Ref.[3]	Ref.[10]	Ref.[11]
Cylinder	0.206	0.190	0.203	0.193	0.202
Error/%		8.4	1.5	6.73	1.98

4.5 The form of the vortex shedding and the vorticity

The form of the vortex shedding at the middle section of fluid flowing around three-dimensional cylinder is shown in Fig.11, and the cloud picture of the pressure at each section is shown in Fig.12. From Fig.11 and Fig.12, the forms of the vortex delivery are not the same at different *xoy*-sections, but it has obvious symmetry about middle section 3 in the spanwise direction. This also proves that the resistance coefficients and the lift coefficients are symmetrical about the middle section.

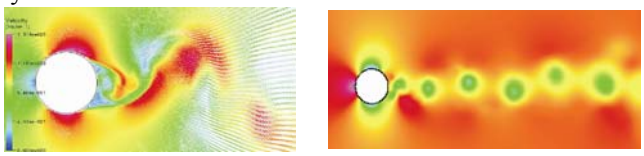

Fig.11 Cloud pictures of the velocity and pressure at the mid section

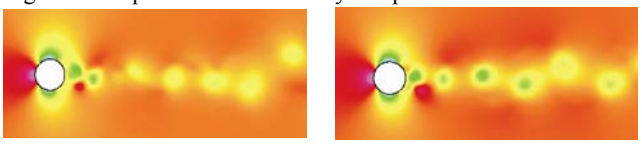

(a) Section 1 (6) Section 2

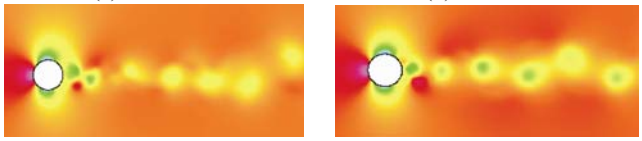

(c) Section 3 (d) Section 4

Fig.12 Cloud pictures of the pressure at each section in the spanwise direction

Vorticity Ω is taken as the variable to draw the iso-surface of the form of the wake's vortex shedding of the three-dimensional flow around the cylinder (Fig.13), and then the vortex tube are obtained to describe the 3-D vortex delivering of the wake of the cylinder. In the spanwise direction of the cylinder, the velocity and phase of the vortex shedding and the strength of vortex at each section are not the same, so the vortex tube is not smooth in the spanwise direction.

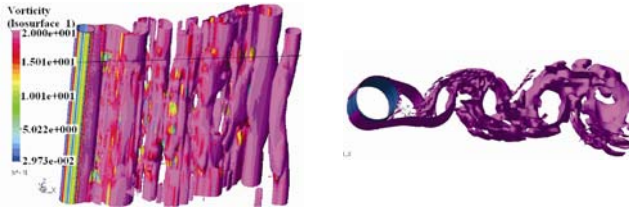

Fig.13 The vortex's isosurface (vorticity=20 m/s)

5 Conclusions

From numerical experimental study of the 3-D flow around the cylinder, the following conclusions are drawn:

1) The stable pressure coefficients at each section in the spanwise direction of the flow around the cylinder do not change significantly, while the fluctuating pressure coefficients change obviously.

2) The resistance coefficients, the lift coefficients and the S_{tr} at each section in the spanwise direction of the flow around the cylinder are symmetrical about the middle section.

3) The vortex tube formed when the vortex of the wake of the cylinder shedding shows twisted phenomena, which suggests that the flow around the cylinder has obvious three-dimensional effects.

4) Research will be carried out in the future: consider the vortex delivery form and the hydrodynamic character of the three-dimensional elastic structures in the uniform flow field; use the parallel computer for many-knot numerical calculation to improve the efficiency of the numerical calculation.

References

[1] ZHANG Zhaoshun, CUI Guixiang, XU Xiaochun. Theory and model of onflow[M]. Beijing: Press of Qinghua University, 2005: 256-160(in Chinese).
[2] WANG Yaling, LIU Yingzhong, MIAO Guoping. Three-dimensional numerical simulation of viscous flow around circular cylinder[J]. Journal of Shanghai Jiaotong University, 2001, 35(19): 1464-1469(in Chinese).
[3] DONG S, KARNIADAKIS G E. DNS of flow past a stationary and oscillating cylinder at *Re*=10000[J]. Journal of Fluids and Structures, 2005(20): 519-531.
[4] BURGER M, SCHMEHL R, KOCH R, et al. DNS of droplet-vortex interaction with a Karman vortex street[J]. Heat and Fluid Flow, 2006(27): 181-191.
[5] CATALANO P, WANG M, IACCARINO G, et al. Numerical simulation of the flow around a circular cylinder at high Reynolds number[J]. Heat and Fluid Flow, 2003(24): 463-469.
[6] LAM K, WANG F K, SO R M C. Three-dimensional nature of vortices in the near wake of a wavy cylinder[J]. Journal of Fluids and Structures, 2004(19): 815-833.
[7] LIN Zonghu. Characteristic of the flow-fluid shed and its engineering application[M]. Beijing: Press of Chemical Industry, 2001(in Chinese).
[8] ESPERANCA P T, JWANDERLEY J B, LEVI C. Validation of a three-dimensional large eddy simulation finite difference method to study vortex induced vibration[C]// Proceedings of 25th International Conference on Offshore Mechanics and Arctic Engineering. Hamburg, 2006: OMAE1003-1987.
[9] PONTAZA J P, CHEN H C. Three-dimensional numerical simulations of circular cylinders undergoing two degree-of-freedom vortex-induced vibrations[C]// Proceedings of 25th International Conference on Offshore Mechanics and Arctic Engineering. Hamburg, 2006: OMAE2006-92052.
[10] GOPALKRISHNAN R. Vortex-induced forces on oscillating bluff cylinder[M]. Cambridge: Massachusetts Institute of Technology, 1993.
[11] NORBERG C. Fluctuating lift on a circular cylinder: review and new measurements[J]. Journal of Fluids and Structures, 2003(17): 57-96.

CHEN Hai-long was born in 1980. He is a candidate for doctor's degree at Harbin Engineering University. His current research interests include fluid-structure interaction, structural dynamics, etc.

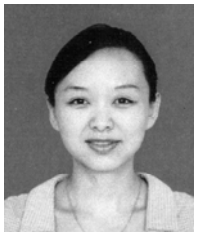

DAI Shao-shi was born in 1976. She is a candidate for doctor's degree at Harbin Engineering University. Her current research interests include fluid-structure interaction, structural dynamics, etc.

LI Jia was born in 1985. She is a candidate for doctor's degree at Harbin Engineering University. Her current research interests include fluid-structure interaction.

基于 LES 方法圆柱绕流三维数值模拟

陈海龙，戴绍士，李　佳，姚熊亮

（哈尔滨工程大学 船舶工程学院，黑龙江 哈尔滨 150001）

摘　要：采用计算流体软件 CFX5 中 large-eddy simulation（LES）模型计算了均匀流场中三维圆柱绕流的水动力特性. 使用有限体积法对三维 N-S 方程进行求解. 数值模拟着重研究了高雷诺数时展向各截面的压力、阻力、升力及涡管特性. 数值计算结果表明：展向各截面柱体受力关于中截面对称且小于二维情况，柱体周围流场呈现明显的三维特性.

关键词：LES 方法；三维圆柱绕流；水动力特性